A Nature Portfolio journal



https://doi.org/10.1038/s43247-025-02356-4

Volcanism records plate thinning driven rift localization in Afar (Ethiopia) since 2-2.5 million years ago

Check for updates

Gianmaria Tortelli ® ^{1,2} ⊠, Anna Gioncada ® ², Carolina Pagli², Dan N. Barfod³, Giacomo Corti ® ⁴, Federico Sani ® ¹, Darren F. Mark³, Ross C. Dymock ® ³, Ermias F. Gebru ® ^{5,6} & Derek Keir ® ^{1,7} ⊠

Magma-rich continental rifting and breakup commonly show complex distributions of volcanism, potentially due to both plume and rifting controls. As such, interpreting the main controls on the spatial evolution of magmatism is debated, as is the point at which continental rifting transitions to oceanic spreading. Here we present new argon-argon dating of 16 lava flows from the Stratoid and Gulf series of the Afar rift. We reconstruct the spatio-temporal evolution of the rift from widely distributed to localised along narrow magmatic segments (i.e., rift localisation). Our results rule out an ocean spreading-like style of rifting. We show that over 2–2.5 million years since the early Pleistocene, the rift progressively narrowed by asymmetric in-rift localisation and propagated along-rift. Concurrently, the mantle partial melting and the crustal magmatic system shallowed. While mantle plume-related elevated temperatures influence overall melt volumes, our results suggest that the rapid and localised changes in plate thinning caused by rifting are the primary control on the spatio-temporal distribution of volcanism.

Magma-rich continental rifts are characterised by large volumes of intruded and erupted igneous rock^{1,2}, in part because rifting and break-up can be associated with a mantle plume^{3–5}. Since mantle melting can result from plume-related thermal anomalies and mantle flow^{6–9}, as well as rift-related decompression melting beneath thinning lithosphere^{10–12}, the evolution of magmatism in space and time is typically complex^{13,14}. Specifically, it has proven challenging to identify when and how highly localised magma intrusion and the associated volcanic systems, typical of the mid-ocean ridge plate boundaries, form during rifting. Consequently, the role played by mantle plumes and plate motion in controlling magmatic activity is still unclear.

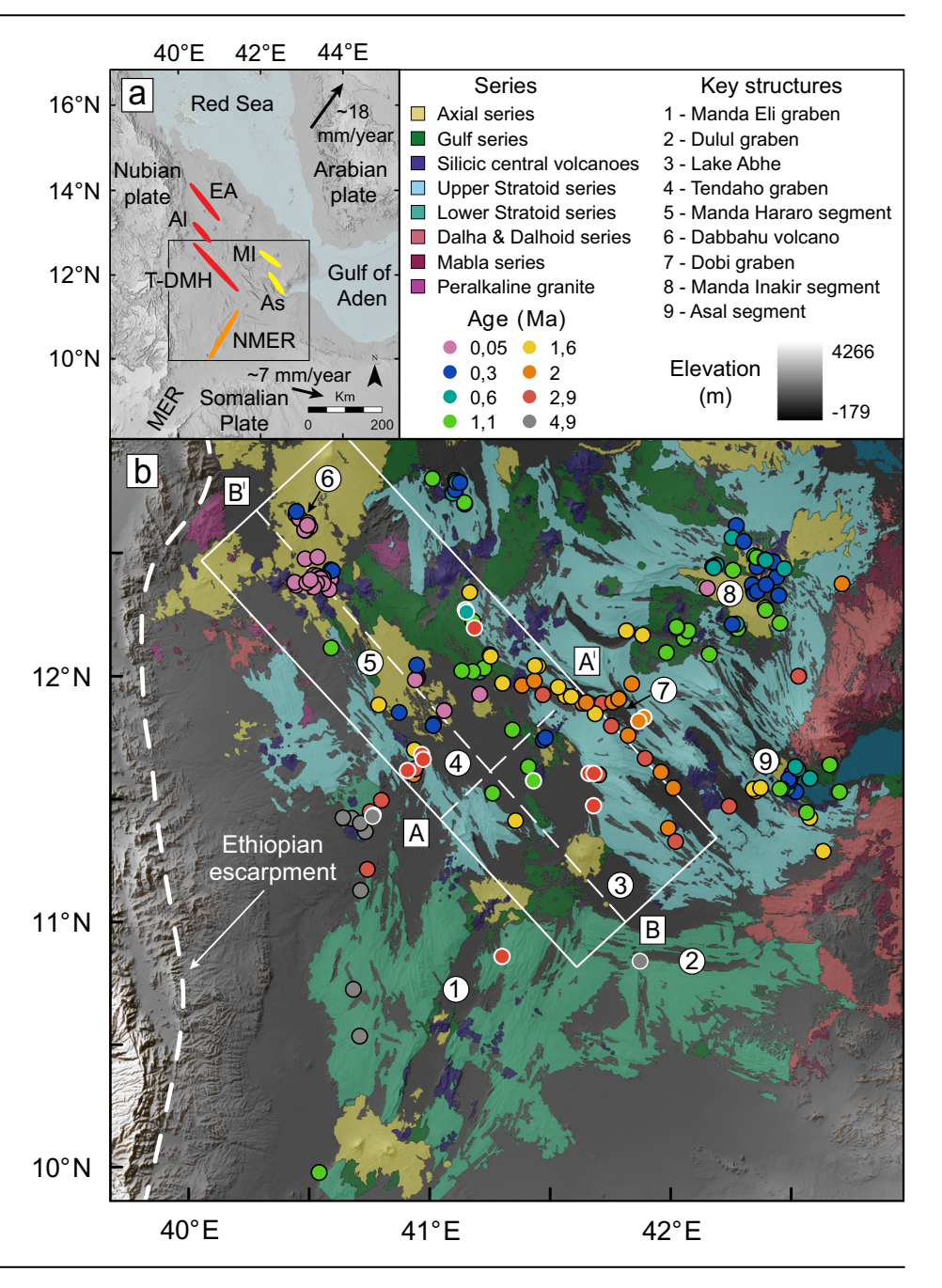
To address these questions, the Afar depression represents a unique place where the spatial and temporal evolution of magmatism during rift evolution can be studied. Rifting in Afar initiated in the Oligocene, toward the end of the Ethiopian-Yemen Flood Basalt volcanism (~31–29 Ma^{15,16}), and the magmatic record of the rift evolution, up to the ongoing activity, is currently exposed within the depression (Fig. 1). The older rift products are the 20–10 Ma silicic Mabla series and 10-4 Ma mainly mafic Dalha and Dalhoid series, outcropping only at the Afar margins¹⁷ (Fig. 1). The central

areas of the depression are instead dominated by the widespread Stratoid series (Fig. 1), consisting of sequences of mostly mafic lava flows reaching 1 km in thickness. In particular, South Afar is dominated by the Lower Stratoid series (LS; 4.5–2.57 Ma¹⁸) while Central Afar by the Upper Stratoid series (US; 2.87–0.88 Ma^{18,19}). In Central Afar, the US was followed by the mostly mafic Gulf series (Gu; 1.11–0.32 Ma^{20,21}; Fig. 1), which erupted principally along the main graben faults²² and marked a decrease in volume with respect to the US¹⁷. Broadly at the same time, several silicic central volcanoes formed throughout Afar (CV; ~2–0.5 Ma^{23,24}). The ongoing localised Axial series (Ax; <1.09 Ma²¹) shows both mafic to silicic central volcanoes and mafic fissural eruptions (Fig. 1), the latter exemplified by the 2005–2010 rifting episode at the Dabbahu-Manda Hararo (DMH) magmatic segment.

The Afar triple junction is formed by the divergent motion between the Arabian, Nubian, and Somalian plates (Fig. 1a). NE-directed rifting between the Arabian and African (i.e., Nubian and Somalian) plates began at $\sim\!29-25~Ma^{16,25}$, forming the Gulf of Aden-Red Sea system and causing extension in Afar 26 . Since at least 11 $Ma^{27,28}$ the rifting has been occurring at a relatively constant rate (16–20 mm/year) and led to the formation of the

¹Dipartimento di Scienze della Terra, Università degli Studi di Firenze, Florence, Italy. ²Dipartimento di Scienze della Terra, Università di Pisa, Pisa, Italy. ³NEIF Argon Isotope Laboratory, Scottish Universities Environmental Research Centre (SUERC), East Kilbride, UK. ⁴Istituto di Geoscienze e Georisorse, Consiglio Nazionale delle Ricerche, Florence, Italy. ⁵Department of Geosciences, University of Fribourg, Fribourg, Switzerland. ⁶School of Earth Sciences, Addis Ababa University, Addis Ababa, Ethiopia. ⁷School of Ocean and Earth Science, University of Southampton, Southampton, UK. ⊠e-mail: gianmaria.tortelli@unifi.it; D.Keir@soton.ac.uk

Fig. 1 | Age distribution of the samples across Afar. a Multi-Directional Hillshade map of Afar with magmatic segments of the Red Sea, Gulf of Aden, and East African Rift, respectively, in red, yellow, and orange. Black arrows represent the spreading vector with respect to a fixed Nubian plate. The black box encloses Southern and Central Afar represented in (b). EA Erta Ale, Al Alayta, T-DMH Tendaho-Dabbahu Manda Hararo, As Asal, MER Main Ethiopian Rift, NMER North Main Ethiopian Rift. b Elevation map of Southern and Central Afar (image source: ESRI) with Multi-Directional Hillshade map in the background (image source: ESRI). On top of the elevation map is shown the geological map of Central and Southern Afar from Tortelli et al.37. All dated samples are coloured based on their age and the new dated samples presented in this work are identified by white rims. The legend in the top right corner refers to (b). The white box identifies the Tendaho-DMH area, enclosing the samples plotted onto across- and along-rift sections (respectively the dashed lines A-A' and B-B') and reported, respectively, in Figs. 2 and 3. New data are provided in Supplementary Data 1 while literature data 18-22, are in Supplementary Data 2.



onshore magmatic segments of the Gulf of Aden (e.g., Asal and Manda Inakir magmatic segments) and Red Sea (e.g., DMH and Erta Ale magmatic segment) rifts, as well as the development of large en-echelon grabens within Central Afar²9 (Fig. 1). Rifting between the Nubian and Somalian plates led instead to the formation of the younger East African Rift (\sim 11 Ma³0), which is currently accommodating extension at \sim 7 mm/year³¹ in a near E-W direction (Fig. 1a).

The crust in Afar is transitional between continental and oceanic in type. It is generally around 25–30 km thick, but locally thins to 15–20 km beneath the current magmatic segments, where substantial melt accumulation occurs^{32,33} (e.g., DMH). Extension in Afar started at ~29–25 Ma, leading to the development of rift margins and marginal basins, marked by the eruption of the Mabla, Dalha, and Dalhoid series (combined during ~20–4.5 Ma)^{16,17,34}. Subsequently, extension has instead been loosely interpreted to be associated with the eruption of the Stratoid series within the depression (~4.5–1.1 Ma)³⁴. The Stratoid series has been described as a pulse of volcanism moving north²⁰, broadly associated with the transition from continental rifting to break-up^{23,35}, or to the first stage of oceanization³⁶.

There are clear age²² and petrological³⁷ variations between the LS and US, which have been linked to different extensional events¹⁷, most likely related to a sudden shift (or jump) of extension from South to Central Afar^{37,38}. Within the US, however, there is ongoing debate regarding their temporal and spatial distribution and link to rift evolution. For example, Stab et al. interpret the broad US spatial distribution to be associated with equally broad extension in Central Afar³⁴, only followed by rift localisation with the onset of the Gu at 1.1 Ma²⁰. In contrast, other authors have recognised younging of the Stratoid toward the centre of the Tendaho graben³⁵ and magnetic stripes akin to classic mid-ocean ridge patterns³⁹, implying a steady-state, ocean spreading-like scenario during which nearly all the extension is accommodated by magmatic accretion. At the same time, a progressive northward propagation of the Stratoid spreading axis has been suggested based on the ages of the Central Afar silicic activity³⁶. In addition to a tectonic control leading to decompression melting^{11,12,39}, a number of studies have suggested that the Afar plume⁴⁰ controls the volcanic activity and rift evolution 41-46. As such, the spatial and temporal distribution of the US and how it relates to the rifting process is still unclear. The lack of a

detailed tectonic framework has also hindered the interpretation of controls on the geochemistry of the US, such as the evolution of the mantle source and subvolcanic plumbing system. Therefore, the mechanisms controlling the spatio-temporal evolution of magmatic activity during rifting in Afar remain poorly resolved⁴⁷.

To address these issues, we provide new ⁴⁰Ar-³⁹Ar data for 16 LS, US, and Gu lava samples from South and Central Afar. We reconstructed the distribution in space and time of the volcanic activity during rifting in Afar. By comparing our observations with models of magma distribution during ocean spreading-like rifting (i.e., the width of the extension zone do not change through time and the magmatism gets progressively younger toward the rift centre at the same rate as rift extension) and rift localisation (i.e., the magmatism youngs toward the rift centre at a faster rate than rift extension due to the width accommodating the extension progressively narrowing through time), we ruled out an ocean spreading-like scenario for the US and identified an asymmetric localisation of the rift in Central Afar. From an initially wide area accommodating diffuse extension (hereafter referred to as Plate Boundary Zone (PBZ)) (i.e., US eruption), the rift became progressively narrower and moved laterally to the current DMH magmatic segment position over the last 2-2.5 Myr. Using geochemical and petrological literature data, we identify a thinned lithosphere associated with a shallower and complex magmatic system for the localised phase. Finally, by combining our reconstruction with chemical data, we suggest that the spatiotemporal distribution of the volcanic activity during rifting is mainly driven by the divergent motion of Arabia and Nubia rather than being plume controlled.

Results

⁴⁰Ar-³⁹Ar geochronology

Our $^{40}\text{Ar-}^{59}\text{Ar}$ dating indicates that the LS ranges from 4.85 ± 0.06 to 2.89 ± 0.03 Ma, the US from 2.58 ± 0.04 to 1.88 ± 0.02 Ma while the Gu spans from 1.07 ± 0.03 to 0.34 ± 0.13 Ma (Supplementary Fig. 1 and Supplementary Data 1). Our analyses extend the lower limit of the known LS range¹⁸ by ~350 kyr. The new ages for the US are also broadly consistent with the literature (2.87–0.88 Ma; Supplementary Data 2), but with our new samples allowing us to redefine the age of the US activity near the Tendaho graben. Our ages of the uppermost (~1250 m) and lowermost (~500 m) flows of the Tendaho graben range from 2.58 ± 0.04 to 2.02 ± 0.02 Ma. These ages indicate the US activity south of Tendaho began earlier than previously thought (2.14 ± 0.06 Ma²²; Supplementary Note 1) and ceased around 2 Ma despite continuing elsewhere until 1.18 ± 0.08 Ma¹⁸. The determined ages of Gu agree with the literature data (1.11-0.32 Ma; Supplementary Data 2). Overall, our new analysis together with literature data (Fig. 1) indicates that the eruptive activity of the last 5 Myr in South and Central Afar was continuous, without a marked temporal gap or overlap between the series.

Temporal evolution models

During rift evolution, the total area accommodating the extension can vary in space and strongly influence the architecture of the rift⁴⁸. Weakness in the lithosphere due to pre-existing structures^{48,49} or thermo-mechanical perturbations^{50,51} (i.e., magma intrusions) can drive strain localisation, causing a decrease in the width of the deformed area accommodating the extension⁵². In contrast, in an ocean spreading-like scenario the area accommodating the extension remains the same through time.

Assuming that each lava sample was emplaced near their eruptive centres, the age variation of the lavas in space can be to a first order indicative of the area accommodating the extension (i.e., PBZ or magmatic segment) and therefore the temporal and spatial evolution of rifting can be evaluated (i.e., ocean spreading-like rifting or rift localisation). This approach has commonly been applied in other magma-rich rifts such as Iceland^{53,54}, much of the mid-ocean ridge system⁵⁵, and other regions of the East African Rift^{56,57}. To define how strain and volcanism evolved in Central Afar, we analysed the ages and spatial distributions of the US, Gu and Ax eruptive products in the Tendaho-DMH area (white box in Fig. 1) where a wide suite

of dating information is now available. Regarding the literature data used in this work, we selected only lava flow samples with an age error smaller than ±0.5 Ma and with a well-constrained sample location (Supplementary Data 2). We excluded the analyses of Barberi et al.⁵⁸ due to discrepancies between some of their ages and ours (see Supplementary Note 1 for a detailed explanation). Furthermore, given the thick exposures of the US and the associated age variation (2.58-2.02 Ma), for the temporal evolution models we selected only the US samples from the uppermost lava flows to avoid age variations related to sampling at different stratigraphic height. Regarding our dataset, the selection was based on our sampling locations, whereas for literature data, it was determined by information provided in the respective manuscripts (Supplementary Data 1 and 2). New and literature analyses were plotted onto two sections, respectively across (Figs. 1(A-A') and 2) and along-rift (Figs. 1'(B-B') and 3), to evaluate the age distribution of lava samples with respect to the DMH magmatic segment. Overall, the volcanic activity gets younger toward the centre of the graben^{20,35} (Fig. 2a) and also toward the NW, where mainly the <1.1 Ma Gu and Ax outcrop (Figs. 1 and 3).

Using the distribution of lava ages across the rift, we evaluate the mechanisms responsible for riftward younging of the volcanic activity. To do this, we calculate the rate at which volcanism gets younger towards the rift centre and compare it with what is expected from ocean spreading-like extension (Fig. 2b) and from rift localisation 59,60 (Fig. 2c), both modelled assuming a constant extension rate over time. For uniform ocean spreadinglike rifting, the position and width of the area accommodating the extension (i.e., the magmatic segment) remain constant through time while the volcanic lavas of the eruptive centre spread away at half of the extension rate equally on both sides of the rift (Fig. 2b). The rate at which the age of volcanic lavas change away from both sides of the rift centre will therefore be the same and their sum equal to the extension rate. Unequal rates between rift sides yet yielding the full extension rate, implies asymmetric ocean spreading-like rifting (Fig. 2b). However, if the observed rate is greater than that expected from ocean spreading-like extension, then localisation from initially broad to more localised volcanism is required (Fig. 2c). In a uniform localisation scenario, as the area accommodating the extension narrows (transitioning from a broad rift to narrow magmatic segment; Fig. 2c) the distance between the volcanic lavas of the older, and spatially wider eruptive products and those of the younger, narrower one increases beyond what is expected from the extension rate alone. As a result, the calculated rate at which the age of the volcanism changes will exceed the extension rate, and its magnitude will depend on the initial width of volcanism and the rate of narrowing. In this scenario, unequal rates between rift sides exceeding the full extension rate imply asymmetric rift localisation (Fig. 2c).

The lavas on the NE side of the Tendaho-DMH area (pale blue crosses in Fig. 2a) have erupted progressively closer to the DMH magmatic segment during the last 2-2.5 Myr, at a rate of 26.7 ± 2.3 mm/year, considerably faster than the half extension rate in Central Afar of ~10 mm/year²⁶. On the SW side of the Tendaho-DMH area (purple crosses in Fig. 2a), the rate is less with respect to the NE side, 11.5 ± 1.5 mm/year, comparable but still slightly higher than the half extension rate of ~10 mm/year. This pattern argues for a localisation of the magmatism that occurred asymmetrically, from NE to SW during the last 2-2.5 Myr. Furthermore, boreholes within the Tendaho graben^{61,62} drilled the young Ax and Gu activity on top of the US, further arguing against an ocean spreading-like scenario. This east-to-west localisation indicates that, at least part of the US PBZ, had to be located east with respect to the DMH magmatic segment. Accordingly, the Moho depth estimates^{33,38} (Supplementary Fig. 2) projected on the same across-rift profile show a thinning of the crust coherent with the younging of the volcanic activity (i.e., toward the centre of the Tendaho graben; Fig. 2a).

Concurrently, all the series plotted on the along-rift profile show younging of the erupted products toward the north during the last 2–2.5 Myr (Fig. 3), indicating that the rift propagated north while localising in-rift. Accordingly, our US ages at the Tendaho graben (lowermost and uppermost flow, 2.58–2.02 Ma) are ~250 kyr older with respect to the northern Dobi graben (intermediate and uppermost flow, 1.93–1.76 Ma²⁰),

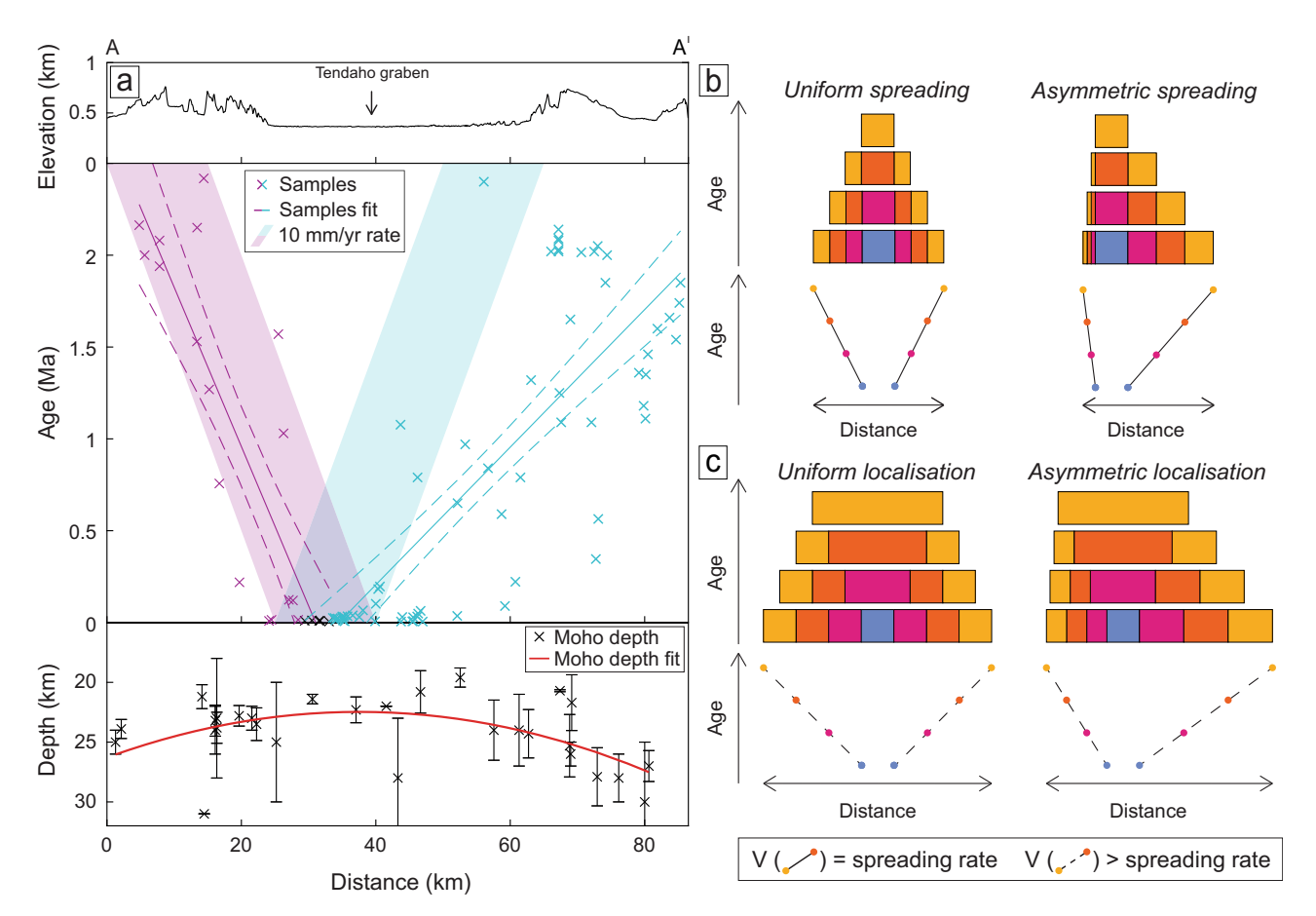


Fig. 2 | Across-rift age distribution of observed and modelled magmatic activity. Observed (a) and modelled (b, c) magmatic activity distribution across rift. a The top image represents the topographic profile of the A–A' across-rift profile (Fig. 1). The middle image shows the ages of the dated samples projected along the A–A' across-rift profile. The colours identify the samples used to fit the linear regression model (solid lines), purple and pale blue crosses are respectively used for the samples located on the SW and NE side of A–A' across-rift profile while the black crosses had been used for both sides. The dashed lines identify the 95% confidence interval of the linear regression. The calculated rates are 11.5 ± 1.5 and 26.7 ± 2.3 mm/year, respectively, for the SW and NE sides. The inclination of each one of the shaded areas identifies half of the Central Afar extension rate (~10 mm/year) spanning broadly the Manda Hararo magmatic segment width. The bottom image shows the estimated Moho depths with the errors projected along the A–A' across-rift profile 33,38 (Supplementary Fig. 2). The estimated depths have been fitted by a polynomial curve (red line) to show the crustal thickness variation. b, c Schematic representations of the

distribution of the eruptive centres areas for both ocean spreading-like rifting (b) and rift localisation (c). Each coloured box indicates the areas accommodating the extension (i.e., the eruptive centres) during a given time period with the total extension rate being kept the same for all the models and through time (the top boxes represent the initial stage while the bottom boxes represent the final stage). Below each one of the box models, a graph shows the hypothetical spatial distribution of eruptive centres at their final stages (bottom boxes of each model) to compare them with the real case (a). b For the uniform ocean spreading-like rifting the width and position of the magmatic segment are fixed. To have asymmetric ocean spreading-like rifting, different spreading rates for the two sides are needed (in the example, it is greater on the right side with respect to the left side). c For the uniform localisation, the width of the Plate Boundary Zone gets narrower toward its centre throughout time. To have asymmetric localisation of the PBZ, different spreading rates are needed (in the example, it is greater on the right side with respect to the left side). See the text for discussion.

indicating that the northward propagation was already occurring during the Upper Stratoid activity. The propagation is also confirmed by boreholes TD-1 and TD-2 of the Tendaho graben^{61,62} where the volcanic deposits are topped by 600/700 m of sedimentary succession while at the borehole TD-3 along the Manda Hararo segment, the volcanic deposits have been found overall continuously up to the surface. This suggests that the magmatic activity ceased at some point after the end of the Upper Stratoid eruption south of Manda Hararo while continuing up to the present day along the magmatic segment itself.

Geochemistry

Changes in the mantle source and in the crustal magmatic system of Tendaho-DMH magmatic activity during rift localisation are investigated using the geochemical composition of both the dated samples (this work and literature data) and the entire suite of the Tendaho-DMH chemical analysis (Fig. 4, Supplementary Fig. 3 and Supplementary Data 2).

Partial melting in the deeper, garnet-bearing portions of the mantle can be identified with respect to the upper, spinel-bearing portions using the highly compatible HREE in $garnet^{63}$ (i.e., Tb_N/Yb_N) for the mafic rocks (MgO > 4 wt%). Melting of a garnet-bearing lower crust or garnet and amphibole fractionation can also influence Tb_N/Yb_N . However, these processes can be excluded due to the low crustal thickness of Central Afar³⁸ and to the absence of garnet and amphibole in the series lavas 37,64,65. The effect on Tb_N/Yb_N due to mantle source heterogeneity can also be ruled out considering the similarity of the trace elements patterns, all corresponding to magma type 3 of Rooney¹⁷ (Supplementary Fig. 4). Changes in Tb_N/Yb_N are therefore related to changes in the depth of melting³⁷. We relate the depth of melting to the lithospheric thinning and exclude the role of mantle potential temperature since no correlation is observed between temperature and Tb_N/ $Yb_N^{7,18}$. The three series show a clear distinction in the Tb_N/Yb_N for both the whole dataset and the group of dated samples only (Fig. 4a). The US ranges mainly at 1.7-1.9, the Gu at 1.6-1.7 and the Ax at 1.3-1.5, indicating a

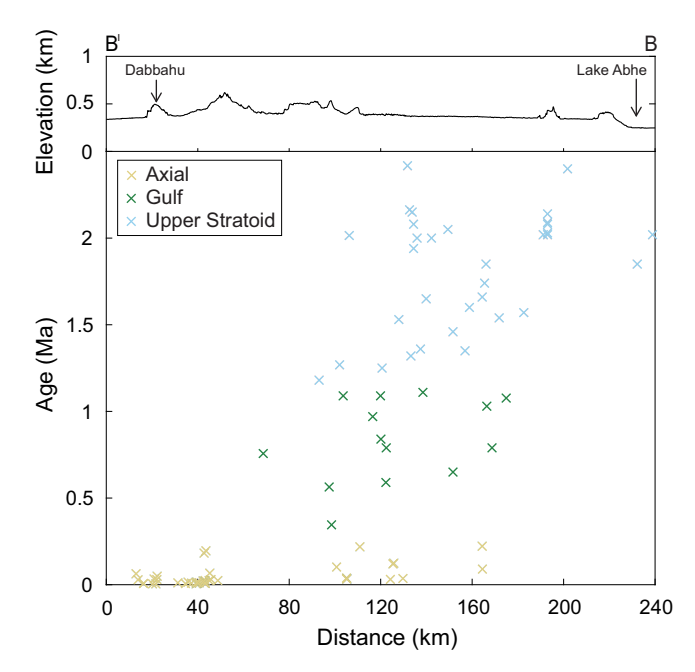


Fig. 3 | Along-rift age distribution of the observed magmatic activity. Topographic profile (top) and sample ages (bottom) of the Tendaho-DMH area projected along the B–B' along-rift profile (Fig. 1). The samples are colour coded according to their series as in Fig. 1b. Overall, a decrease in age toward north-west for each series is observed.

shallowing of the partial melting column, and therefore a thinning of the lithosphere, from the US to Gu to Ax.

The degree of magmatic evolution of the samples (i.e., MgO wt%) and the overall stationing depth of the magma of the three series have been used to reconstruct the changes of the magmatic system architecture during rifting. In order to focus on the variations of the fissural magmatic activity systems, we did not take into consideration analyses of the central volcanoes (i.e., Dabbahu). A variation of the MgO content between the series is observed for both the whole dataset and the group of dated samples (Fig. 4b). The US have a unimodal distribution of moderately evolved lavas (4-6 MgO wt%) while the Gu are dominated by a slightly more mafic composition (5-7 MgO wt%) with respect to the US (Fig. 4b). The Ax have instead a clear bimodal distribution with mafic (8-9 MgO wt%) and moderately evolved (5-6 MgO wt%) lavas (Fig. 4b). Furthermore, these variations are associated with changes in the stationing depth. Along the magmatic segments, the Ax plumbing system is arranged in stacked sills and vertical dikes^{66,67} from the Moho level^{68,69} to the upper crust⁷⁰⁻⁷³ (up to 2 km depth) while US and Gu are stationed mainly in the middle-lower crust⁷⁴ (10-18 km). These observations indicate a transition from a deep and overall stable magmatic system buffering the moderately differentiated US composition to a more complex one for the Ax, where magma can either reach and differentiate at shallower levels or more rapidly rise to the surface emplacing more primitive lavas.

Discussion

The spatio-temporal reconstruction of the volcanic activity carried out in this work indicates that, over the last 2–2.5 Myr, the rift in Central Afar asymmetrically localised in-rift (Fig. 2) while propagating toward the NW (Fig. 3), marking the progressive transition from the initially widespread US eruptions to the current narrow magmatic segment. This suggests that the rift localisation process was more protracted than previously thought and started well within the US period, rather than being limited to the most recent Gu and Ax periods. We therefore interpret that the US volcanism is strongly linked to rifting and tracks the progressive localisation process of the rift. Our reconstruction indicates that the US are associated with continental rifting^{23,35} as their spatio-

temporal distribution is not consistent with an ocean spreading-like style of extension⁷⁵. Furthermore, the US distributes in space and time coherently with the subsequent Gu and Ax activity, identifying a progressive localisation process and arguing for a similar mechanism controlling the evolution of the volcanic activity. We therefore suggest that, as for the more recent volcanic activity^{56,73}, the distribution of the US eruption is controlled by the locus of plate thinning caused by the rifting of Arabia and Nubia rather than by a major plume control.

The interpretation of rift focusing is fully consistent with geochemical evidence for progressive shallowing of the melting column interpreted as thinning of the lithosphere (Fig. 4a) together with the development of a complex magmatic system (Fig. 4b) forming shallow magma chambers^{70–72} in a thinned crust^{33,38} (Fig. 2a). The deeper partial melting and magma storage of the US with respect to the Gu and Ax suggests the US are associated with continental rifting, as these depths are not consistent with an ocean spreading-like scenario^{13,76}. During rifting, the effect of magmatism^{77,78}, stretching^{79,80} and metasomatism^{81,82} can weaken the lithosphere¹⁴ while melt and volatiles rising from the mantle can weaken the crusts^{83,84}, explaining the observed shallowing of partial melting and magma chambers⁸⁵. We therefore suggest that, during continental rifting, at least part of the shallowing of partial melting occurs during the rift localisation with broadly simultaneous changes in the crustal structure.

Seismic images of the mantle beneath East Africa suggest the mantle plume is spatially much broader than the rift, as it is clearly imaged beneath the adjacent Ethiopian and Arabian plateaus86, with back simulation of mantle convection through time showing limited change on the scale of Afar over the last 5 Myr⁸⁷. While the elevated mantle temperatures associated with the mantle plume^{7,88} help to facilitate mantle melting, petrological models of melt production show that the rift-related plate thinning is still likely required for the upwelling asthenosphere to cross the solidus and produce a substantial amount of partial melt⁸⁹. We therefore interpret the plume to be a ubiquitous feature of the wider region, but with the rifting above it being the primary control on the locus of magmatism. Such an interpretation is consistent with Afar mantle chemistry and mantle potential temperature. The US has indeed a mantle source very similar to the older LS, Dalhoid and Dalha series¹⁷ and to the younger Gu and Ax series^{17,18,90}, with little variations of the Afar plume component⁴⁰ occurring during partial melting. Similarly, the mantle potential temperature remains similar for LS, US, Gu and Ax^{7,18} indicating no thermal perturbation of the mantle source. We therefore suggest the US eruption is not related to an increase of the plume activity with respect to the more recent volcanic activity as variations in a rising plume would have led to marked variations in both mantle temperature and chemistry^{91,92}.

Our reconstruction agrees with analogue and numerical models of rift evolution showing alternating periods of rift propagation and localisation of the volcanic activity of and progressively shallower depths of sill emplacement while the rift matures. Geological and geophysical observations in Afar also corroborate our model, such as magmatic segments propagating NW^{24,29,95,96}, the Manda Hararo segment shifting westward and the presence of the young Ma' Alalta magmatic segment NW of DMH and the deeper melting column in the earlier stage of the rift. The divergent motion between Arabia and Nubia advocated in this work as the main driver of rift localising agrees with numerical models showing that asymmetric plate motion above a waning mantle plume can lead to migration of the locus of extension. Moreover, our reconstruction is consistent with the Stratoid being associated to extensional events on the primary control on volcanism being rift related adiabatic decompression melting 11,100.

The north-westward evolution of the rift pointed out in this study is coherent with the en-echelon distribution of grabens caused by the counter-clockwise rotation of the Danakil Block in Central Afar²⁹. Our reconstruction, along with the associated graben distribution, supports the linkage of the Gulf of Aden-Red Sea system taking place in Central Afar¹⁰¹. Furthermore, the observed northward propagation of the rift in Central Afar oppose

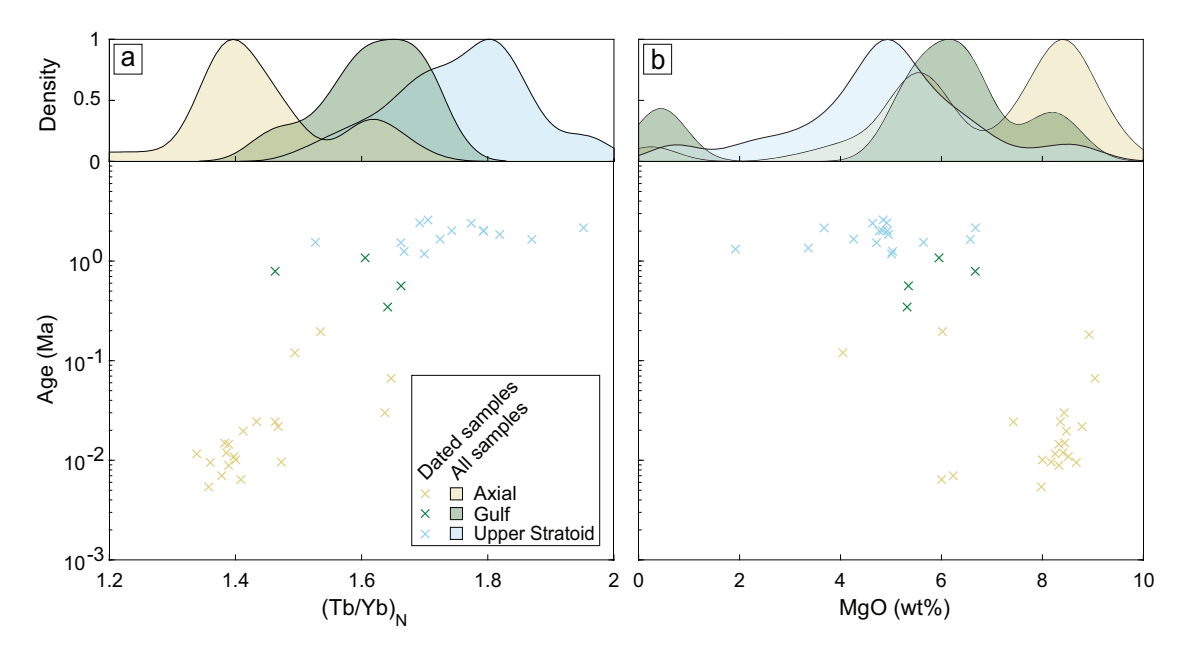


Fig. 4 | Chemical variations of the Afar magmatic activity according to their ages. Mantle- and crustal-related chemical variations of the lava flow samples erupted in the Tendaho-DMH area. a The Tb/Yb normalised to the chondritic values (McDonough and Sun, 1995)¹¹⁰ for the mafic samples (MgO > 4 wt%) has been used as a proxy of the depth of the melting column. The upper figure represents the normalised kernel density estimation of all samples according to their respective series while

below are reported only the dated samples. The samples are colour coded according to their series as in Fig. 1b. **b** Same as (**a**) using the MgO wt% of the samples to evaluate changes in the melt degree of evolution and therefore variations in the magmatic system architecture among the series. See the text for discussion. New data are provided in Supplementary Data 1 while literature data 182337748897,111-114 in Supplementary Data 2.

to the southward propagation of the offshore Red Sea rift, arguing in favour of the regional-scale distinction between the onshore rift of Central Afar (i.e., the Afar rift²⁹) and the offshore Red Sea rift²⁹.

This work provides precise temporal constraints regarding the process of rift localisation which can help to improve the still poorly defined temporal reconstruction of the rift to drift transition 102,103 (<10 Ma). In particular, during magma-rich rifting, the transition from broad to narrow rifting and consequent formation of a magmatic segment takes place relatively rapidly (2–2.5 Myr). Furthermore, this work provides insight into the long-standing debate regarding the role of mantle plume vs plate tectonics during rifting 10,47,104,105 . We showed that, while the elevated temperature associated with the mantle plume can favour melt generation, variations in the distribution and volumes of the volcanic activity during rift evolution, up to small-scale flood basalts-like eruptions, are primarily controlled by tectonic processes such as localised thinning of the lithosphere.

Methods Sampling

Sixteen lava flow samples (4 LS, 9 US and 3 Gu; Fig. 1) from a sampling campaign in 2020 and the Afar Repository of the University of Pisa were selected based on their petrographic and geochemical analysis ^{37,74} in order to avoid any evidence of alteration. The selection of samples aimed to cover as much of South and Central Afar as possible, and to temporally constrain the eruptive period of the LS and US lava flows by dating the visible lowermost flows of the Dulul and Tendaho graben escarpments. The ⁴⁰Ar-³⁹Ar dating was carried out on the groundmass for all samples and on plagioclase phenocrysts for the silicic sample (AF20-69a; Supplementary Data 1). Samples preparation and analyses were carried out at the NEIF Argon Isotope Laboratory at the Scottish Universities Environmental Research Centre (SUERC).

Sample preparation

Initially, heavily weathered outer portions of each sample were removed using a Controls 32-D0536/A saw and the relatively fresh interiors were screened using a petrographic microscope to identify any signs of alteration in the groundmass and to evaluate the feasibility of analysis. Suitable whole

rock samples were then crushed in a Pulverisette 1 jaw crusher producing fragments ~1-5 mm, which were then fed into a Pulverisette 13 disc mill to further reduce the size before finally being sieved to produce a 250–500 µm separate. A hand magnet was used to remove any metal particles left over from the crushing process, before being rinsed in deionized water to remove any adhering dust and other loose fragments. The separates were then leached in an ultrasonic bath, for 20-30 min in a 2.5 M HNO₃ solution to remove alteration phases which is then followed by a 3 M HCl solution to remove olivine phenocrysts. These leaching steps are repeated as many times as is necessary to remove the unwanted materials. The samples were then cleaned in deionized water to remove dust, dried at temperature <75 °C and sieved to remove possible fragments created by comminution during leaching. By repeated passage in a Frantz Isodynamic Magnetic Barrier Separator, non-magnetic phenocrysts and alteration products were separated from the magnetic lava groundmass, and feldspar phenocrysts were separated from the lava groundmass. Lastly, each lava sample has had ~400 mg of homogenous and unaltered groundmass hand-picked under a binocular microscope. For the feldspar separates, once obtained, they were further processed with the Frantz to isolate any remaining melt inclusionrich feldspar grains and magnetic groundmass from the non-magnetic, melt inclusion-free, feldspar grains. The selected feldspar grains were then further leached in a 1 M HF solution for 3-5 min to remove adhering glass, cleaned in deionized water and dried at temperature <75 °C. The last step was to ensure all the feldspar grains were inclusion-free by hand-picking under a binocular microscope.

Sample analysis

Lava groundmass and feldspar samples and neutron flux monitors were packaged into 7-pit Al discs, sealed and then stacked in quartz tubes with the relative positions of packets precisely measured for later reconstruction of neutron flux gradients. The sample package was irradiated in the Oregon State University Triga reactor's Cadmium Lined In-Core Irradiation Tube (CLICIT) facility. The international 40 Ar- 39 Ar standard, Alder Creek sanidine, 1.1891 \pm 0.0008 Ma (\pm 1 σ 106) was used to monitor 39 Ar production and establish neutron flux values (*J*) for the samples. Gas was extracted from samples in a step-wise fashion, heated using a Teledyne-Cetac Fusions mid-

infrared (10.6 µm) CO₂ laser with a non-Gaussian, uniform energy profile and a 3.5 mm beam diameter. The samples were housed in a doubly pumped ZnS window laser cell and loaded into a copper planchette containing four 2.6 cm² square wells. Liberated argon was purified of active gases, (e.g., CO₂, H₂O, H₂, N₂, CH₄) using three Zr-Al getters; one at 18 °C and two at 400 °C. Data were collected on a Thermo Scientific ARGUS VI multi-collector mass spectrometer in static collection (non-peak hopping) mode. Time-intensity data are regressed to t_0 with second-order polynomial fits to the data. Blank corrections employed the average value and standard deviation of multiple blanks bracketing and interspersed with sample and air standard runs. Mass discrimination was monitored daily, both between and within sample runs, by comparison to running-average values of an air standard. All data are blank, interference and mass discrimination corrected using the MassSpec software package (MassSpec, authored by Al Deino, Berkeley Geochronology Centre, Version 8.149). Decay constants and corrections (Supplementary Data 1) were selected after Renne et al. 107.

Most of the samples were run in duplicate and a plateau age calculated for each analysis. Age and uncertainty were calculated using the mean weighted by the inverse variance of each step. The isochrons were calculated using the plateau steps to determine the composition of the trapped component and isochron age. The plateau age was accepted if (I) it consists of at least five consecutive age steps indistinguishable within 2σ uncertainty, (II) it comprises a minimum of 60% of the total ³⁹Ar released, (III) it is concordant with the isochron age at the 2σ level, and (IV) has a ⁴⁰Ar-³⁶Ar trapped component indistinguishable from air (298.56 ± 0.62) at the 2σ level (Supplementary Data 1). A number of analyses show a small excess of 40 Ar*, i.e., a non-atmospheric trapped component. In these instances, the isochron age is preferred as the best estimate of the timing of emplacement and may be interpreted as a maximum age (see Supplementary Note 2 for details). The replicated plateau ages overlap in age at the 2σ level. However, in many cases, combining plateau steps from replicates to calculate a composite plateau generated excess scatter such that mean square weighted deviation exceeded the critical value at a given N. It is for this reason that we choose the most precise determination in a set of replicated analyses that satisfy the plateau acceptance criteria above as the best estimate of emplacement age. All the data are provided in Supplementary Data 1 and Supplementary Fig. 1. All ages are presented herein at 2σ uncertainty level.

Data availability

All data that support the findings of this work are presented in the paper and/or in the Supplementary Material and deposited in Zotero public repository at: https://doi.org/10.5281/zenodo.15197563.

Received: 20 September 2024; Accepted: 5 May 2025; Published online: 21 May 2025

References

- White, J. D. L., Bryan, S. E., Ross, P.-S., Self, S. & Thordarson, T. in Studies in Volcanology: the Legacy of George Walker (eds Thordarson, T., Self, S., Larsen, G., Rowland, S. K. & Höskuldsson, Á.) 291–321 (Geological Society of London, 2009).
- Holbrook, W. S. & Kelemen, P. B. Large igneous province on the US Atlantic margin and implications for magmatism during continental breakup. *Nature* 364, 433–436 (1993).
- White, R. & McKenzie, D. Magmatism at rift zones: The generation of volcanic continental margins and flood basalts. *J. Geophys. Res.* Solid Earth 94, 7685–7729 (1989).
- Courtillot, V., Jaupart, C., Manighetti, I., Tapponnier, P. & Besse, J. On causal links between flood basalts and continental breakup. Earth Planet. Sci. Lett. 166, 177–195 (1999).
- Koppers, A. A. P. et al. Mantle plumes and their role in Earth processes. *Nat. Rev. Earth Environ.* 2, 382–401 (2021).
- Nelson, W. R., Furman, T., van Keken, P. E., Shirey, S. B. & Hanan, B. B. OsHf isotopic insight into mantle plume dynamics

- beneath the East African rift system. Chem. Geol. 320–321, 66–79 (2012).
- Rooney, T. O., Herzberg, C. & Bastow, I. D. Elevated mantle temperature beneath East Africa. Geology 40, 27–30 (2012).
- Buiter, S. J. H. & Torsvik, T. H. A review of Wilson Cycle plate margins: a role for mantle plumes in continental break-up along sutures? *Gondwana Res.* 26, 627–653 (2014).
- Holbrook, W. S. et al. Mantle thermal structure and active upwelling during continental breakup in the North Atlantic. *Earth Planet. Sci. Lett.* 190, 251–266 (2001).
- Cawood, P. A., Strachan, R. A., Pisarevsky, S. A., Gladkochub, D. P. & Murphy, J. B. Linking collisional and accretionary orogens during Rodinia assembly and breakup: implications for models of supercontinent cycles. *Earth Planet. Sci. Lett.* 449, 118–126 (2016).
- Rychert, C. A. et al. Volcanism in the Afar rift sustained by decompression melting with minimal plume influence. *Nat. Geosci.* 5, 406–409 (2012).
- Gallacher, R. J. et al. The initiation of segmented buoyancy-driven melting during continental breakup. Nat. Commun. 7, 13110 (2016).
- Armitage, J. J. et al. Upper mantle temperature and the onset of extension and break-up in Afar, Africa. Earth Planet. Sci. Lett. 418, 78–90 (2015).
- Brune, S. et al. Geodynamics of continental rift initiation and evolution. Nat. Rev. Earth Environ. 4, 235–253 (2023).
- Hofmann, C. et al. Timing of the Ethiopian flood basalt event and implications for plume birth and global change. *Nature* 389, 838–841 (1997).
- Wolfenden, E., Ebinger, C., Yirgu, G., Renne, P. R. & Kelley, S. P. Evolution of a volcanic rifted margin: Southern Red Sea, Ethiopia. Geol. Soc. Am. Bull. 117, 846 (2005).
- Rooney, T. O. The cenozoic magmatism of East Africa: Part IV The terminal stages of rifting preserved in the northern East African rift system. *Lithos* 360–361, 105381 (2020).
- Feyissa, D. H. et al. Transition from plume-driven to plate-driven magmatism in the evolution of the main Ethiopian rift. *J. Petrol.* 60, 1681–1715 (2019).
- Zumbo, V., Féraud, G., Vellutini, P., Piguet, P. & Vincent, J. First 40Ar/ 39Ar dating on Early Pliocene to Plio-Pleistocene magmatic events of the Afar - Republic of Djibouti. *J. Volcanol. Geotherm. Res.* 65, 281–295 (1995).
- Lahitte, P., Gillot, P., Kidane, T., Courtillot, V. & Bekele, A. New age constraints on the timing of volcanism in central Afar, in the presence of propagating rifts. J. Geophys. Res. Solid Earth 108, 2001JB001689 (2003).
- Manighetti, I. et al. Propagation of rifting along the Arabia-Somalia Plate Boundary: into Afar. J. Geophys. Res. Solid Earth 103, 4947–4974 (1998).
- Kidane, T. et al. New paleomagnetic and geochronologic results from Ethiopian Afar: block rotations linked to rift overlap and propagation and determination of a ~2 Ma reference pole for stable Africa. J. Geophys. Res. Solid Earth 108, 2001JB000645 (2003).
- Barberi, F. & Santacroce, R. The Afar Stratoid Series and the magmatic evolution of East African rift system. *Bull. Soc. Géol. Fr.* S7-XXII, 891–899 (1980).
- Lahitte, P., Gillot, P.-Y. & Courtillot, V. Silicic central volcanoes as precursors to rift propagation: the Afar case. *Earth Planet. Sci. Lett.* 207, 103–116 (2003).
- Watchorn, F., Nichols, G. J. & Bosence, D. W. J. in Sedimentation and Tectonics in Rift Basins Red Sea:- Gulf of Aden (eds Purser, B. H. & Bosence, D. W. J.) 165–189 (Springer Netherlands, 1998).
- McClusky, S. et al. Kinematics of the southern Red Sea–Afar triple junction and implications for plate dynamics. *Geophys. Res. Lett.* https://doi.org/10.1029/2009GL041127 (2010).

- ArRajehi, A. et al. Geodetic constraints on present-day motion of the Arabian plate: implications for Red Sea and Gulf of Aden rifting. Tectonics 29, 2009TC002482 (2010).
- Reilinger, R. & McClusky, S. Nubia–Arabia–Eurasia plate motions and the dynamics of Mediterranean and Middle East tectonics. Geophys. J. Int. 186, 971–979 (2011).
- Rime, V., Foubert, A., Ruch, J. & Kidane, T. Tectonostratigraphic evolution and significance of the Afar depression. *Earth Sci. Rev.* 244, 104519 (2023).
- Wolfenden, E., Ebinger, C., Yirgu, G., Deino, A. & Ayalew, D.
 Evolution of the northern Main Ethiopian rift: birth of a triple junction.
 Earth Planet. Sci. Lett. 224, 213–228 (2004).
- Stamps, D. S. et al. A kinematic model for the East African rift. Geophys. Res. Lett. https://doi.org/10.1029/2007GL032781 (2008).
- Hammond, J. O. S. et al. The nature of the crust beneath the Afar triple junction: evidence from receiver functions. Geochem. Geophys. Geosyst. https://doi.org/10.1029/2011GC003738 (2011).
- Ahmed, A. et al. Across and along-strike crustal structure variations of the western Afar margin and adjacent plateau: insights from receiver functions analysis. J. Afr. Earth Sci. 192, 104570 (2022).
- Stab, M. et al. Modes of rifting in magma-rich settings: tectonomagmatic evolution of Central Afar. Tectonics 35, 2–38 (2016).
- Acocella, V., Abebe, B., Korme, T. & Barberi, F. Structure of tendaho graben and manda hararo rift: implications for the evolution of the Southern Red Sea propagator in central Afar. *Tectonics* 27, 2007TC002236 (2008).
- Varet, J. Geology of Afar (East Africa) (Springer International Publishing, 2018).
- Tortelli, G. et al. Constraints on the magma source and rift evolution from geochemistry of the Stratoid flood basalts (Afar, Ethiopia). Geochem. Geophys. Geosyst. 23, e2022GC010434 (2022).
- Hammond, J. O. S. et al. The nature of the crust beneath the Afar triple junction: evidence from receiver functions: crustal structure beneath Afar, Ethiopia. Geochem. Geophys. Geosyst. https://doi. org/10.1029/2011GC003738 (2011).
- Bridges, D. L., Mickus, K., Gao, S. S., Abdelsalam, M. G. & Alemu, A. Magnetic stripes of a transitional continental rift in Afar. Geology 40, 203–206 (2012).
- Rooney, T. O. et al. Upper mantle pollution during Afar plume–continental rift interaction. *J. Petrol.* 53, 365–389 (2012).
- Koulakov, I. Yu. Structure of the Afar and Tanzania plumes based on the regional tomography using ISC data. *Dokl. Earth Sci.* 417, 1287–1292 (2007).
- Meshesha, D. & Shinjo, R. Rethinking geochemical feature of the Afar and Kenya mantle plumes and geodynamic implications. J. Geophys. Res. Solid Earth https://doi.org/10.1029/2007JB005549 (2008)
- Nyblade, A. A. in Volcanism and Evolution of the African Lithosphere (eds Beccaluva, L., Bianchini, G. & Wilson, M.) Ch. 3 (Geological Society of America, 2011).
- 44. Castillo, P. R., Liu, X. & Scarsi, P. The geochemistry and Sr-Nd-Pb isotopic ratios of high ³He/⁴He afar and MER basalts indicate a significant role of the African superplume in EARS magmatism. *Lithos* 376–377, 105791 (2020).
- Rajaonarison, T. A., Stamps, D. S., Naliboff, J., Nyblade, A. & Njinju, E. A. A geodynamic investigation of plume-lithosphere interactions beneath the East African rift. *J. Geophys. Res. Solid Earth* 128, e2022JB025800 (2023).
- Sreenidhi, K. S., Betts, P. G., Radhakrishna, M. & Armit, R. Influence of lateral plume channel on the evolution of rift arms of the Afar triple junction: constraints from 3-D gravity interpretation. *J. Geophys.* Res. Solid Earth 128, e2023JB026791 (2023).
- Issachar, R., Haas, P., Augustin, N. & Ebbing, J. Rift and plume: a discussion on active and passive rifting mechanisms in the Afro-

- Arabian rift based on synthesis of geophysical data. Solid Earth 15, 807–826 (2024).
- Corti, G. Evolution and characteristics of continental rifting: analog modeling-inspired view and comparison with examples from the East African rift system. *Tectonophysics* 522–523, 1–33 (2012).
- Dunbar, J. A. & Sawyer, D. S. Continental rifting at pre-existing lithospheric weaknesses. *Nature* 333, 450–452 (1988).
- Buck, W. R. in Rheology and Deformation of the Lithosphere at Continental Margins (eds Karner, G. D., Taylor, B., Driscoll, N. W. & Kohlstedt, D. L.) 1–30 (Columbia University Press, 2004).
- Buck, W. R. The role of magma in the development of the Afro-Arabian rift system. Geol. Soc. Lond. Spec. Publ. 259, 43–54 (2006).
- Corti, G. et al. Transition from continental break-up to punctiform seafloor spreading: how fast, symmetric and magmatic. *Geophys. Res. Lett.* 30, 2003GL017374 (2003).
- 53. Tegner, C., Brooks, C. K., Duncan, R. A., Heister, L. E. & Bernstein, S. ⁴⁰Ar-³⁹Ar ages of intrusions in East Greenland: rift-to-drift transition over the Iceland hotspot. *Lithos* 101, 480–500 (2008).
- Martin, E. et al. Geodynamics of rift–plume interaction in Iceland as constrained by new ⁴⁰Ar/³⁹Ar and in situ U–Pb zircon ages. *Earth Planet. Sci. Lett.* 311, 28–38 (2011).
- Goldstein, S. J., Murrell, M. T., Janecky, D. R., Delaney, J. R. & Clague, D. A. Geochronology and petrogenesis of MORB from the Juan de Fuca and Gorda ridges by ²³⁸U–²³⁰Th disequilibrium. *Earth Planet. Sci. Lett.* **107**, 25–41 (1991).
- Ferguson, D. J. et al. Constraining timescales of focused magmatic accretion and extension in the Afar crust using lava geochronology. *Nat. Commun.* 4, 14–16 (2013).
- Michon, L., Famin, V. & Quidelleur, X. Evolution of the East African rift system from trap-scale to plate-scale rifting. *Earth Sci. Rev.* 231, 104089 (2022).
- Barberi, F., Ferrara, G., Santacroce, R. & Varet, J. Structural evolution of the Afar Triple Junction. *Afar Depress. Ethiop.* 1, 38–54 (1975).
- Buck, W. R. Modes of continental lithospheric extension. J. Geophys. Res. Solid Earth 96, 20161–20178 (1991).
- Brun, J. P. Narrow rifts versus wide rifts: inferences for the mechanics of rifting from laboratory experiments. *Philos. Trans. R.* Soc. Lond. Ser. Math. Phys. Eng. Sci. 357, 695–712 (1999).
- Gianelli, G. et al. Water–rock interaction and hydrothermal mineral equilibria in the Tendaho geothermal system. J. Volcanol. Geotherm. Res. 86, 253–276 (1998).
- Battistelli, A., Yiheyis, A., Calore, C., Ferragina, C. & Abatneh, W. Reservoir engineering assessment of Dubti geothermal field, Northern Tendaho Rift, Ethiopia. *Geothermics* 31, 381–406 (2002).
- Wang, K., Plank, T., Walker, J. D. & Smith, E. I. A mantle melting profile across the basin and range, SW USA. *J. Geophys. Res. Solid Earth* 107, ECV 5-1–ECV 5-21 (2002).
- Field, L., Blundy, J., Calvert, A. & Yirgu, G. Magmatic history of Dabbahu, a composite volcano in the Afar rift, Ethiopia. *Geol. Soc. Am. Bull.* 125, 128–147 (2013).
- Medynski, S. et al. Magmatic cycles pace tectonic and morphological expression of rifting (Afar depression, Ethiopia). Earth Planet. Sci. Lett. 446, 77–88 (2016).
- Hammond, J. O. S. Constraining melt geometries beneath the Afar depression, Ethiopia from teleseismic receiver functions: the anisotropic H-κ stacking technique. *Geochem. Geophys. Geosyst.* 15, 1316–1332 (2014).
- Chambers, E. L., Harmon, N., Rychert, C. A. & Keir, D. Variations in melt emplacement beneath the northern East African rift from radial anisotropy. *Earth Planet. Sci. Lett.* 573, 117150 (2021).
- Desissa, M. et al. A mantle magma reservoir beneath an incipient mid-ocean ridge in Afar, Ethiopia. Nat. Geosci. 6, 861–865 (2013).

- La Rosa, A. et al. Simultaneous rift-scale inflation of a deep crustal sill network in Afar, East Africa. Nat. Commun. 15, 4287 (2024).
- Grandin, R. et al. Sequence of rifting in Afar, Manda-Hararo rift, Ethiopia, 2005–2009: time-space evolution and interactions between dikes from interferometric synthetic aperture radar and static stress change modeling. *J. Geophys. Res. Solid Earth* https:// doi.org/10.1029/2009JB000815 (2010).
- Didana, Y. L., Thiel, S. & Heinson, G. Magnetotelluric imaging of upper crustal partial melt at Tendaho graben in Afar, Ethiopia. Geophys. Res. Lett. 41, 3089–3095 (2014).
- Hamling, I. J. et al. Geodetic observations of the ongoing Dabbahu rifting episode: new dyke intrusions in 2006 and 2007. *Geophys. J. Int.* 178, 989–1003 (2009).
- Wright, T. J. et al. Magma-maintained rift segmentation at continental rupture in the 2005 Afar dyking episode. Nature 442, 291–294 (2006).
- Tortelli, G. et al. From melt- to crystal-rich magmatic systems during rift localization: insights from mineral chemistry in central Afar (Ethiopia). Contrib. Mineral. Petrol. 179, 87 (2024).
- Müller, R. D., Sdrolias, M., Gaina, C. & Roest, W. R. Age, spreading rates, and spreading asymmetry of the world's ocean crust. Geochem. Geophys. Geosyst.9, 2007GC001743 (2008).
- Moore, C., Wright, T., Hooper, A. & Biggs, J. The 2017 eruption of Erta'Ale volcano, Ethiopia: insights into the shallow axial plumbing system of an incipient Mid-Ocean Ridge. *Geochem. Geophys.* Geosyst. 20, 5727–5743 (2019).
- Havlin, C., Parmentier, E. M. & Hirth, G. Dike propagation driven by melt accumulation at the lithosphere–asthenosphere boundary. *Earth Planet. Sci. Lett.* 376, 20–28 (2013).
- 78. Bialas, R. W., Buck, W. R. & Qin, R. How much magma is required to rift a continent? *Earth Planet. Sci. Lett.* **292**, 68–78 (2010).
- Chenin, P., Schmalholz, S. M., Manatschal, G. & Karner, G. D. Necking of the lithosphere: a reappraisal of basic concepts with thermo-mechanical numerical modeling. *J. Geophys. Res. Solid Earth* 123, 5279–5299 (2018).
- 80. Petri, B. et al. Thinning mechanisms of heterogeneous continental lithosphere. *Earth Planet. Sci. Lett.* **512**, 147–162 (2019).
- 81. Pilet, S., Baker, M. B. & Stolper, E. M. Metasomatized lithosphere and the origin of alkaline lavas. *Science* **320**, 916–919 (2008).
- Rooney, T. O., Brown, E. L., Bastow, I. D., Arrowsmith, J. R. & Campisano, C. J. Magmatism during the continent – ocean transition. *Earth Planet. Sci. Lett.* 614, 118189 (2023).
- Ebinger, C. J. et al. Crustal structure of active deformation zones in Africa: implications for global crustal processes. *Tectonics* 36, 3298–3332 (2017).
- Muirhead, J. D. et al. Evolution of upper crustal faulting assisted by magmatic volatile release during early-stage continental rift development in the East African rift. Geosphere 12, 1670–1700 (2016).
- Hopper, E. et al. Preferential localized thinning of lithospheric mantle in the melt-poor Malawi rift. *Nat. Geosci.* 13, 584–589 (2020).
- 86. Civiero, C. et al. Small-scale thermal upwellings under the northern East African rift from S travel time tomography. *J. Geophys. Res. Solid Earth* **121**, 7395–7408 (2016).
- Moucha, R. & Forte, A. M. Changes in African topography driven by mantle convection. *Nat. Geosci.* 4, 707–712 (2011).
- 88. Ferguson, D. J. et al. Melting during late-stage rifting in Afar is hot and deep. *Nature* **499**, 70–73 (2013).
- McKenzie, D. & Bickle, M. J. The volume and composition of melt generated by extension of the lithosphere. *J. Petrol.* 29, 625–679 (1988).
- Alene, M. et al. Geochemistry of Woranso–Mille Pliocene basalts from west-central Afar, Ethiopia: implications for mantle source characteristics and rift evolution. *Lithos* 282–283, 187–200 (2017).

- Carter, E. J. et al. Volcanic tempo driven by rapid fluctuations in mantle temperature during large igneous province emplacement. *Earth Planet. Sci. Lett.* 644, 118903 (2024).
- Natali, C. et al. High-MgO lavas associated to CFB as indicators of plume-related thermochemical effects: the case of ultra-titaniferous picrite-basalt from the northern Ethiopian-Yemeni plateau. Gondwana Res. 34, 29–48 (2016).
- Beutel, E., Van Wijk, J., Ebinger, C., Keir, D. & Agostini, A. Formation and stability of magmatic segments in the Main Ethiopian and Afar rifts. Earth Planet. Sci. Lett. 293, 225–235 (2010).
- Ferrante, G., Rivalta, E. & Maccaferri, F. Spatio-temporal evolution of rift volcanism controlled top-down by a deepening graben. *Earth Planet. Sci. Lett.* 629, 118593 (2024).
- Sani, F., Ghinassi, M., Papini, M., Oms, O. & Finotello, A. Evolution of the northern tip of Afar triangle: inferences from the Quaternary succession of the Dandiero — Massawa area (Eritrea). *Tectonophysics* 717, 339–357 (2017).
- Dumont, S. et al. Rifting processes at a continent-ocean transition rift revealed by fault analysis: example of Dabbahu-Manda-Hararo Rift (Ethiopia). *Tectonics* 38, 190–214 (2019).
- 97. Medynski, S. et al. Stability of rift axis magma reservoirs: spatial and temporal evolution of magma supply in the Dabbahu rift segment (Afar, Ethiopia) over the past 30 kyr. *Earth Planet. Sci. Lett.* **409**, 278–289 (2015).
- 98. Tortelli, G. et al. Evidence of active magmatic rifting at the Ma'Alalta volcanic field (Afar, Ethiopia). *Bull. Volcanol.* **83**, 38 (2021).
- Mather, B. et al. Spreading ridge migration enabled by plume-ridge de-anchoring. *Nat. Commun.* 15, 8934 (2024).
- De Chabalier, J.-B. & Avouac, J.-P. Kinematics of the Asal rift (Djibouti) determined from the deformation of Fieale volcano. Science 265, 1677–1681 (1994).
- Eagles, G., Gloaguen, R. & Ebinger, C. Kinematics of the Danakil microplate. *Earth Planet. Sci. Lett.* 203, 607–620 (2002).
- Ding, W. et al. Lateral evolution of the rift-to-drift transition in the South China Sea: evidence from multi-channel seismic data and IODP Expeditions 367&368 drilling results. *Earth Planet. Sci. Lett.* 531, 115932 (2020).
- Larsen, H. C. et al. Rapid transition from continental breakup to igneous oceanic crust in the South China Sea. *Nat. Geosci.* 11, 782–789 (2018).
- 104. Foulger, G. R. *Plates vs Plumes: A Geological Controversy* (Wiley, 2011).
- Zhang, N., Dang, Z., Huang, C. & Li, Z.-X. The dominant driving force for supercontinent breakup: plume push or subduction retreat?. Geosci. Front. 9, 997–1007 (2018).
- Niespolo, E. M., Rutte, D., Deino, A. L. & Renne, P. R. Intercalibration and age of the Alder Creek sanidine 40Ar/39Ar standard. *Quat. Geochronol.* 39, 205–213 (2017).
- 107. Renne, P. R., Balco, G., Ludwig, K. R., Mundil, R. & Min, K. Response to the comment by W.H. Schwarz et al. on "Joint determination of 40K decay constants and ⁴⁰Ar*/⁴⁰K for the Fish Canyon sanidine standard, and improved accuracy for ⁴⁰Ar/³⁹Ar geochronology" by P.R. Renne et al. (2010). *Geochim. Cosmochim. Acta* 75, 5097–5100 (2011).
- Courtillot, V. et al. Episodic spreading and rift propagation: new paleomagnetic and geochronologic data from the Afar Nascent passive margin. J. Geophys. Res. Solid Earth 89, 3315–3333 (1984).
- Daoud, M. A. et al. Young rift kinematics in the Tadjoura rift, western Gulf of Aden, Republic of Djibouti. *Tectonics* https://doi.org/10. 1029/2009TC002614 (2011).
- McDonough, W. F. & Sun, S. S. The composition of the Earth. Chem. Geol. 120, 223–253 (1995).
- 111. Ayalew, D., Pik, R., Bellahsen, N., France, L. & Yirgu, G. Differential fractionation of rhyolites during the course of crustal extension,

- Western Afar (Ethiopian rift). Geochem. Geophys. Geosyst. 20, 571–593 (2019).
- 112. Barberi, F., Ferrara, G., Santacroce, R., Treuil, M. & Varet, J. A transitional basalt-pantellerite sequence of fractional crystallization, the Boina Centre (Afar Rift, Ethiopia). *J. Petrol.* 16, 22–56 (1975).
- Barrat, J. A. et al. Geochemistry of basalts from Manda Hararo, Ethiopia: LREE-depleted basalts in Central Afar. *Lithos* 69, 1–13 (2003).
- Ferguson, D. J. et al. Recent rift-related volcanism in Afar, Ethiopia.
 Earth Planet. Sci. Lett. 292, 409–418 (2010).

Acknowledgements

The research is part of the PhD of G.T., funded by the 2017 PRIN projectprotocol MIUR: 2017P9AT72 PE10. G.T. acknowledges support by the Tuscany Regional PhD Course in Earth Sciences. The 40Ar-39Ar dating was supported by the 2017 PRIN project-protocol MIUR: 2017P9AT72 PE10. D.K. is partially supported through NERC grant NE/L013932/1. We are grateful to Maria Laura Balestrieri and Carolina Ortiz Guerrero for handling the manuscript, and to Antoine Delaunay and the two anonymous reviewers for their insightful comments, which greatly improved the quality of the paper. We thank Alfredo Battistelli and the managers of Ethiopian Electric Power (EEP) geothermal activities for their availability to share the Geology section of the final report of Tendaho Geothermal Project (Aquater, 1996). We thank Tyrone Rooney for the constructive discussion on this work prior to publication. We thank the colleagues of the Addis Ababa University and the Ethiopian and Afar Regional Governments for their support and for granting permission to conduct sampling. We thank the drivers of the rental agency Ethioder, and the local policeman and guides of several woredas for their support and logistic help in organising and conducting the February 2020 campaign.

Author contributions

G.T., D.K. and C.P. designed the project. G.T., D.K., G.C. and E.G. organised the fieldwork. G.T., E.G., D.K., G.C., F.S. and A.G. conducted the field trip and helped with sample collection. G.T., D.B., D.M. and R.D. prepared the samples for analysis and performed the ⁴⁰Ar-³⁹Ar analyses and the data corrections. G.T. and C.P. compiled the literature dataset. G.T., A.G., D.K. and C.P. participated in the interpretation of the data. G.T. wrote the initial

version of the manuscript and prepared the figures. All authors contributed to the editing and revision of the manuscript and figures.

Competing interests

The authors declare no competing interests.

Additional information

Supplementary information The online version contains supplementary material available at https://doi.org/10.1038/s43247-025-02356-4.

Correspondence and requests for materials should be addressed to Gianmaria Tortelli or Derek Keir.

Peer review information Communications Earth & Environment thanks Antoine Delaunay and the other anonymous reviewer(s) for their contribution to the peer review of this work. Primary handling editors: Maria Laura Balestrieri, Carolina Ortiz Guerrero. A peer review file is available.

Reprints and permissions information is available at http://www.nature.com/reprints

Publisher's note Springer Nature remains neutral with regard to jurisdictional claims in published maps and institutional affiliations.

Open Access This article is licensed under a Creative Commons Attribution 4.0 International License, which permits use, sharing, adaptation, distribution and reproduction in any medium or format, as long as you give appropriate credit to the original author(s) and the source, provide a link to the Creative Commons licence, and indicate if changes were made. The images or other third party material in this article are included in the article's Creative Commons licence, unless indicated otherwise in a credit line to the material. If material is not included in the article's Creative Commons licence and your intended use is not permitted by statutory regulation or exceeds the permitted use, you will need to obtain permission directly from the copyright holder. To view a copy of this licence, visit http://creativecommons.org/licenses/by/4.0/.

© The Author(s) 2025